I&EC research
Industrial & Engineering Chemistry Research

pubs.acs.org/IECR

Article

Modeling, Optimization, and Techno-Economic Analysis of Bipolar Membrane Electrodialysis for Direct Air Capture Processes

Francesco Sabatino,* Matteo Gazzani, Fausto Gallucci, and Martin van Sint Annaland

Cite This: *Ind. Eng. Chem. Res.* 2022, 61, 12668−12679

Read Online

ACCESS | Metrics & More | Article Recommendations | Supporting Information

ABSTRACT: Bipolar membrane electrodialysis (BPMED) could allow for the complete electrification of direct air capture (DAC) technologies. In this work, we have modeled and optimized two DAC processes based on different electrodialysis cell designs. The technical assessment has been complemented by a detailed economic analysis, showing the advantages but also the current shortcomings of this technology and pathways for advancement. A minimum energy demand of 24 MJ $kg_{CO_2}^{-1}$ has been estimated for the base-case scenario, a result comparable to what has been reported for other liquid-scrubbing DAC technologies. Several solutions to further abate power consumption have been reviewed, with the most promising case providing a 29% reduction. Membrane cost and performance are currently the main limiting factors. In a scenario where cheaper membranes with better performance are assumed to be available, total costs below $250 $ton_{CO_2}^{-1}$ may be feasible, making BPMED a viable fully electrified alternative to other technologies requiring natural gas.

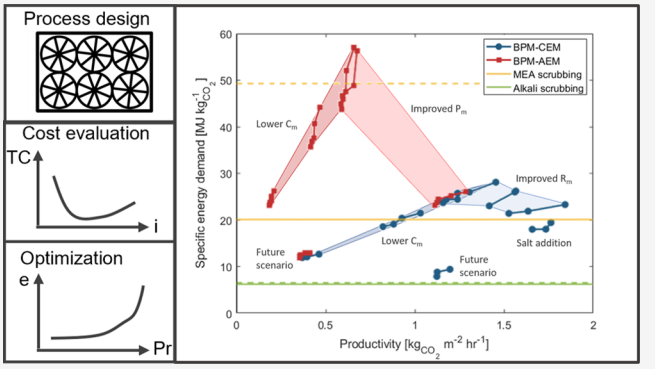

1. INTRODUCTION

As a consequence of COVID-19, global CO_2 emissions fell by 6.4% in 2020, when many countries underwent a lockdown. While this decrease is remarkable, it is still well below the needed cut of 7.6% per year in the next decade to prevent global warming above 1.5 °C.[1] Within this context, artificial removal of CO_2 from the atmosphere, that is direct air capture (DAC), is to be expected to become a pivotal technology to tackle hard-to-avoid emissions. DAC possesses a few key advantages over other natural or technological approaches for carbon removal. First, DAC plants are modular and scalable and, compared to other carbon dioxide removal (CDR) technologies such as bioenergy with carbon capture and storage, do not require extensive land area. Moreover, DAC does not call for uncertain geoengineering measures, and the CDR it provides is easily quantified.[2] To efficiently capture CO_2 from such a diluted source as air, both liquid and solid sorbents can be adopted.[3] Originally proposed by Zeman in 2007,[4] wet scrubbing with aqueous alkali hydroxide solutions is perhaps the DAC technology that most resembles conventional CO_2 removal processes (e.g., from natural gas or flue gas). In fact, Carbon Engineering is a DAC company working on the development of a plant capable of extracting 1 $Mton_{CO_2}$ $year^{-1}$ from air. In this process, CO_2 is captured in the form of carbonate by an aqueous solution of KOH. The clever design of the absorption units, adapted from cooling tower technologies, provides optimal contact between air and solvent. However, solvent regeneration and CO_2 release are carried out through a complex and energy-intensive thermochemical cycle that requires temperatures exceeding 900 °C and therefore involves the oxy-combustion of a fuel, typically assumed to be natural gas.[5]

Electrochemical alternatives for the recovery of CO_2 from the solvent solution have also been investigated.[6] These technologies can be easily integrated with renewable energy sources, as the only energy input is electricity. Electrochemical methods are generally based on the concept of pH swing, where the pH of the solvent is shifted between basic and acidic conditions to either capture or release CO_2.[7] The equilibrium of carbon dioxide in water is controlled by the pH; CO_2 is outgassed from an acidic solution and absorbed by basic ones.[8] Electrochemical technologies can however differ in the way the pH swing is generated. Shu et al. experimentally demonstrated a continuous process using a H_2-recycling electrochemical cell;[9] the protons produced from the oxidation of H_2 at the anode acidify the CO_2-rich solution, while at the cathode the solvent is regenerated through the production of hydroxides. The authors have measured an energy consumption of 7.89 MJ $kg_{CO_2}^{-1}$ and regeneration of up to 59% of the capture capacity

Received: March 16, 2022
Revised: July 10, 2022
Accepted: July 25, 2022
Published: August 9, 2022

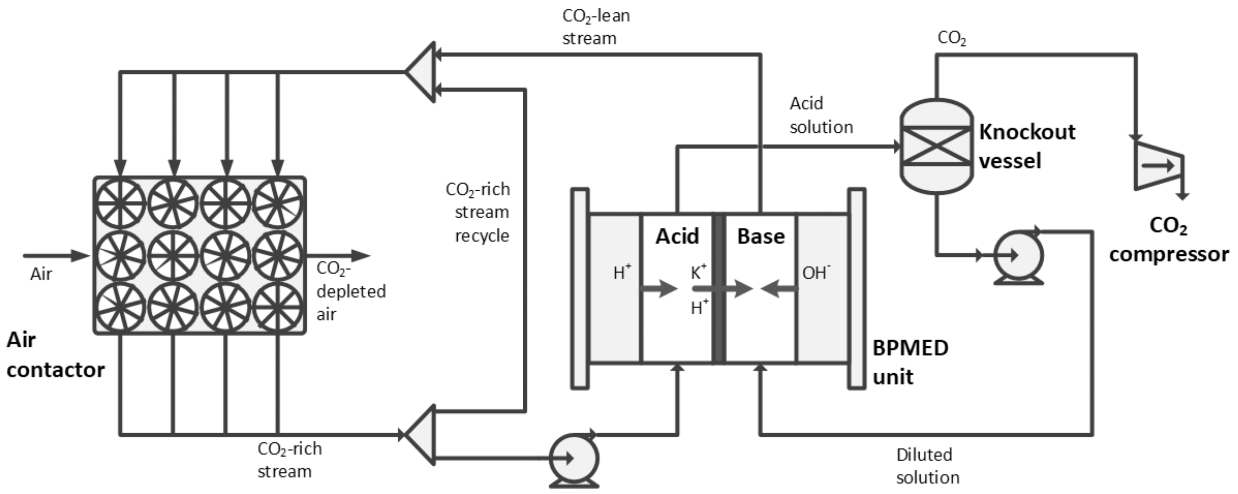

Figure 1. Schematic representation of the DAC process adopting the CEM cell configuration for the BPMED.

of the solvent. Zhou et al. reported a process using a $Ca(OH)_2$ solvent;[10] neutral water electrolysis is employed to create a pH gradient across the cell, with acidic conditions in the anode compartment and basic conditions at the cathode. Here, the Ca^{2+} cations react with OH^- to regenerate $Ca(OH)_2$. This concept has been investigated, and optimal conditions have been assessed through experiments.

Bipolar membrane electrodialysis (BPMED) is a particularly interesting alternative as it can dissociate water and thus produce a pH swing with a minimum voltage drop of 0.829 V, which is 2.5 times lower than that required by electrolysis.[7] BPMED has been thoroughly investigated experimentally,[11−13] and different process concepts aimed at reducing its energy demand have been proposed.[14,15] A BPMED unit is composed of an alternating series of bipolar membranes (BPMs) and ion-exchange membranes (IEMs). When a sufficient voltage is applied, the BPM dissociates water into H^+ and OH^-, thus inducing a pH gradient. The design of the BPMED cell is of fundamental importance as it affects the entire DAC process in several ways. As the pH range required for this application is limited, two-compartment configurations are the simplest working option. This arrangement involves the lowest number of membranes and, therefore, a lower cell electrical resistance.[16] Furthermore, there are two possible BPMED configurations depending on whether a cation-exchange membrane (CEM) or an anion-exchange membrane (AEM) is adopted. The IEM separates the base compartment receiving the influx of hydroxides produced by the BPM from the acid one which collects the protons.

In a previous work,[17] we assessed a DAC process adopting the BPM−AEM cell arrangement using experimental data reported in the literature[11,14] to fit the efficiency of the BPMED unit and assess the overall process performance. The high total process cost of \$773 $ton_{CO_2}^{-1}$ we estimated is in part due to a suboptimal process configuration and in part to the inadequate permselectivity of AEMs. In this regard, a BPM−CEM cell would provide room for improvement in addition to superior conductivity and mechanical stability.[18] We also found that BPMED, which is currently a quite expensive technology, weighs heavily on the economics of the process.

With this work, we extend and further improve our analysis of the application of BPMED for solvent regeneration and CO_2 recovery by exploring a more efficient process configuration and different strategies for reduction of the energy demand. In this work, we have assessed two different BPMED processes thorough rigorous process modeling and optimization. Moreover, we propose a novel strategy for reduction of the energy demand, namely, addition of an inert salt. In this regard, this publication provides a significant novelty with respect to the existing literature.[13,15,17] While in our previous work we relied on the experimental data published by Eisaman et al.[11,14] to determine the efficiency of the BPMED unit, here the process performance is estimated with thermodynamic models and parameters from commercially available industrial-scale BPMED technologies. In this work, we model and optimize two DAC processes combining the proven wet-scrubbing technology developed by Carbon Engineering with BPMED, carrying out a consistent assessment of both cell configurations. The processes are simulated in Aspen Plus using a combination of detailed rate-based and equilibrium blocks. The processes are evaluated on the grounds of energy demand (MJ $kg_{CO_2}^{-1}$) and BPMED productivity (kg_{CO_2} m^{-2} h^{-1}), which are the key performance indicators and proxies of operating and capital costs, respectively. Moreover, to assess the full potential of this technology, a rigorous multiobjective optimization is carried out on the basis of these two performance indicators. Finally, the technical results are used to perform an economic assessment, thus identifying the main contributions to the total process cost.

The manuscript is organized as follows. In Section 2 the methodology adopted is described in detail. Section 3 reports the main results for both configurations, starting from the BPM−CEM one, while in Section 4 a comparison with other liquid scrubbing DAC technologies is provided. Finally, in Section 5 the main conclusions are outlined.

2. PROCESS DESCRIPTIONS AND METHODOLOGY

2.1. Process Schemes. The cell configuration affects not only the BPMED unit design but also the entire solvent regeneration cycle. On the other hand, the extraction of CO_2 from ambient air does not depend on the regeneration layout and is fixed as described by Sabatino et al.[19]

Carbon dioxide is captured in the air contactor unit through chemical absorption in an aqueous solution of KOH, where it reacts to produce K_2CO_3 according to the following reactions

https://doi.org/10.1021/acs.iecr.2c00889
Ind. Eng. Chem. Res. 2022, 61, 12668−12679

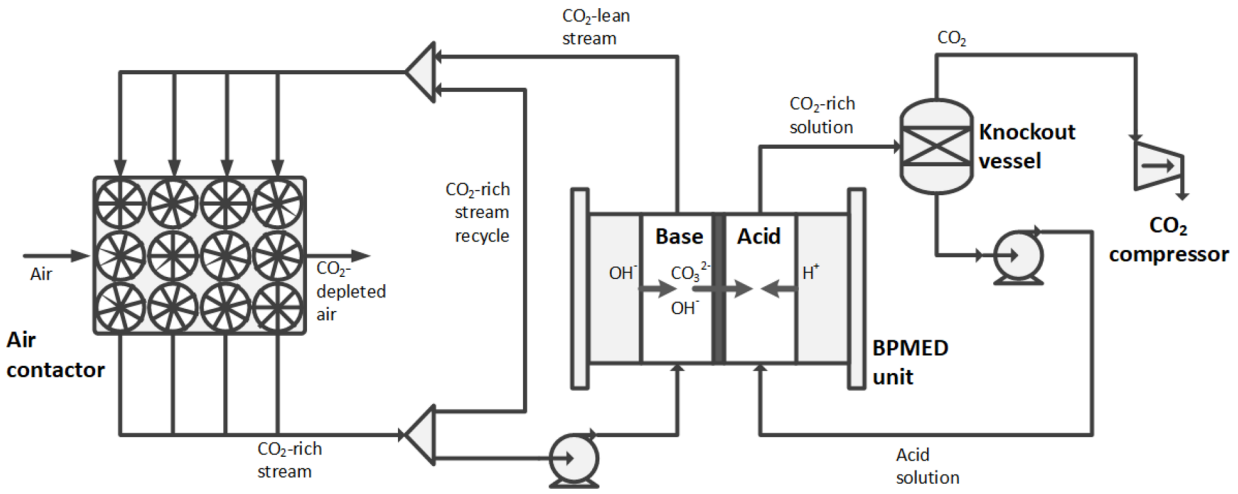

Figure 2. Schematic representation of the DAC process adopting the AEM cell configuration for the BPMED.

$$CO_{2(g)} \rightleftharpoons CO_{2(aq)} \quad (1)$$

$$CO_{2(aq)} + OH - \rightleftharpoons HCO_3^- \quad (2)$$

$$HCO_3^- \rightleftharpoons CO_3^{2-} + H+ \quad (3)$$

The overall reaction can be represented by

$$CO + 2KOH \rightleftharpoons H_2O + K_2CO_3 \quad (4)$$

The air contactor unit has been extensively described by Carbon Engineering.[5,20,21] The design is inspired by commercial humid-air cooling towers, which are devised to efficiently bring very large quantities of ambient air into contact with water on a packing material. Details regarding the modeling of the air contactor can be found in detail elsewhere.[17,19]

In the process adopting the BPM−CEM cell configuration, the CO_2-rich stream is fed to the acid compartment, as shown in Figure 1. The influx of protons (H^+) produced from the electrodissociation of water inside the bipolar membrane reduces the pH of the CO_2-rich stream, thus converting the carbonate ions (CO_3^{2-}) to dissolved carbon dioxide according to the backward reactions 2 and 3. At the same time, K^+ and possibly H^+ ions are transported across the CEM to the base compartment. The BPMED unit is operated at high pressure to limit the release of gaseous CO_2 (reaction 1). In fact, the formation of bubbles could increase the resistivity of the cell and therefore the energy demand associated with solvent regeneration.[14] CO_2 is finally recovered in the knockout vessel, where an expansion induces a drastic reduction in solubility. The liquid stream, which is very diluted in KOH and CO_2, is fed to the base compartment, where it receives the influx of K^+ from the acidic compartment and OH^- from the bipolar membrane.

The regeneration layout for the BPM−AEM cell configuration process, which is represented in Figure 2, is different.

In this case, the CO_2-rich stream is fed to the base compartment while an aqueous solution of phosphoric acid (H_3PO_4) circulates between the acid compartment and the knockout vessel. Carbon dioxide, which is present almost exclusively in the form of CO_3^{2-}, and OH^- are transported through the AEM to the acid compartment. Here, because of the low pH, carbonate ions (CO_3^{2-}) are converted to dissolved CO_2.

For both configurations, only part of the CO_2-rich stream is regenerated, while most of it is recycled back to the air contactor. This affects the CO_2 capture efficiency negatively, as a solvent with a lower absorption capacity is fed to the air contactor. On the other hand, a much higher CO_2 loading can be achieved, which is a crucial aspect for efficient operation of BPMED.[17]

The two processes have been modeled in Aspen Plus (version 11), which provides accurate estimation of all of the relevant thermodynamic properties via the electrolyte NRTL method. The acid and base compartments are assumed to be perfectly mixed and in physical and chemical equilibrium. The IEMs are taken to be ideal with respect to similarly charged ions, i.e., they are permeable only to oppositely charged ions. However, they are modeled as not perfectly selective with respect to the ions of interest in these processes (i.e., K^+ and H^+ for CEMs, CO_3^{2-} and OH^- for AEMs). The flows of similarly charged counterions A and B through an IEM are calculated on the basis of the permselectivity, which is defined as

$$P_B^A = \frac{t_A/t_B}{C_A/C_B} \quad (5)$$

$$t_i = \frac{|z_i|J_i}{\sum_i^n |z_i|J_i} = \frac{|z_i|J_i}{J} \quad (6)$$

where t_i and C_i are the transport number and the ion concentration in the acidic compartment of component i, respectively. For the BPM−CEM cell configuration process, P_B^A is not a decisive parameter as the concentration of protons in the acid compartment is generally orders of magnitude lower than the concentration of K^+. In this case, the permselectivity is assumed to be equal to 2 based on literature data.[22] On the other hand, the concentrations of the OH^- and CO_3^{2-} ions in the base compartment of the BPM−AEM cell are typically comparable. Therefore, for this configuration, estimation of a realistic value for the permselectivity is of paramount importance. On the basis of the experimental results reported by Eisaman et al.,[14] a value of 0.2 has been selected for the permselectivity. Additional details regarding the modeling of the BPMED unit are reported in the Supporting Information.

https://doi.org/10.1021/acs.iecr.2c00889
Ind. Eng. Chem. Res. 2022, 61, 12668−12679

2.2. Energy Demand of BPMED. The power consumption of the BPMED unit $\dot{W}_{BPMED}$ is driven by the voltage drop across a single cell[23]

$$\dot{W}_{BPMED} = iSn_{cell}E_{cell} \tag{7}$$

$$E_{cell} = iR_{cell} + E_{BP} \tag{8}$$

where R_{cell} is the specific resistance of a single cell and E_{BP} is the water-splitting potential of the bipolar membrane, which is 0.829 V for a $\Delta(pH)$ of 14. R_{cell} is the sum of the resistances of the acidic and basic compartments and the IEM and BPM separating them

$$R_{cell} = R_{base} + R_{IEM} + R_{BPM} + R_{acid} \tag{9}$$

The resistivity for the BPM is assumed to be 5.2×10^{-4} Ω m^2, while for the anion- and cation-exchange membranes R is considered to be 4.1×10^{-4} and 1.5×10^{-4} Ω m^2, respectively.[17] The conductivity of an electrolyte solution is a function of the concentration of each of the dissolved ionic species. A proper estimate of the conductivity for both solutions is necessary for an accurate assessment of the energy demand of BPMED. For the electrolyte components of interest, correlations have been fitted from experimental data[24] and are reported in the Supporting Information. The overall conductivity of the compartments is calculated as the sum of the individual contribution of each of the n electrolyte components present in either acid or base solution

$$K = \sum_{i}^{n} k_i \tag{10}$$

For the acid compartment, the release of gaseous CO_2 in the form of bubbles should also be accounted for.[12,17] As gas bubbles are perfect insulators, their presence could cause a reduction of the effective membrane area and consequently an increase in the overall resistance of the acid compartment. This effect is described with the model proposed by Meredith and Tobias[25]

$$K_{acid}^{mp} = K_{acid}\frac{8(2 - \phi_{CO_2})(1 - \phi_{CO_2})}{(4 + \phi_{CO_2})(4 - \phi_{CO_2})} \tag{11}$$

with K_{acid}^{mp} being the conductivity of the multiphase acid solution and ϕ_{CO_2} the gas volume fraction of CO_2 in the acid compartment. In spite of its simplicity, this approach provides accurate results.[17]

2.3. Design of the BPMED Unit. The current density i is the major operating parameter for the BPMED unit as it greatly affects its energy demand and productivity. The specific energy demand tends to increase with increasing current density due to ohmic losses, as described by eq 7. On the other hand, a low current density is detrimental to the process rate, as the molar flow rate J of electrolyte crossing the IEM is proportional to i

$$J = \frac{iS}{F} \tag{12}$$

where S is the membrane area and F is Faraday's constant (96 485.3 s A mol^{-1}). Energy demand and productivity are related to operational expenditures (OPEX) and capital expenditures (CAPEX), respectively. Therefore, there is a clear trade off between the energy consumption and the process rate, meaning that an optimum current density can be identified on the basis of the total costs.[17] Since an optimization can be easily performed on economic grounds, i is not contemplated as a design variable.

The design of the BPMED unit is carried out according to the following procedure. The ion flow rate J and its composition are determined through process simulation in Aspen Plus. Subsequently, a bottom-up, detailed economical evaluation is performed in Matlab to estimate the total process cost as a function of the current density. Details regarding the methodology of this economic assessment and the main assumptions adopted for evaluation of the total costs are reported in the Supporting Information. Once the optimum current density is determined, the total membrane area required is evaluated using eq 12. Thus, the energy demand and productivity are computed.

The economic analysis is used not only to carry out the design of the BPMED unit but also to identify the main cost drivers of both processes and to compare their potential with alternative technologies.

2.4. Multiobjective Optimization. The optimal performance of the two DAC systems has been identified through a multiobjective optimization. In processes adopting BPMED to recover CO_2 from alkali solutions, the membranes and overall energy demand are generally the main drivers of the total cost.[17] For this reason, two objectives have been selected, the productivity of the BPMED unit and the overall electrical consumption. These are competing objectives, meaning that the optimal performance is represented by the Pareto front, a region where the productivity can only be increased at the cost of a higher energy demand. The optimization problem is defined as

$$\begin{aligned} &\underset{x}{\text{minimize}}(-pr,\ e) \\ &\text{subject to } \Phi \geq \Phi_{spec} \end{aligned} \tag{13}$$

where x are decision variables, Φ is the purity, and Φ_{spec} is the required minimum purity (here assumed to 95%, as for CO_2 storage applications). The productivity pr is calculated as

$$pr = \frac{\dot{m}_{CO_2}}{S_m} \tag{14}$$

where $\dot{m}_{CO_2}$ is the mass flow rate of CO_2 recovered from the rich stream and S_m is the total membrane area of the BPMED units. The air contactor generally contributes to a large share of the overall cost of a DAC process.[5,19,26] It has been shown, however, that BPMED can easily have a bigger influence on the economics due to the steep price of BPMs.[17] Therefore, maximizing pr should guarantee not only the best results for the BPMED but also the best economic outcome for the entire process.

The specific energy demand e is calculated with the following equation

$$e = \frac{1}{\dot{m}_{CO_2}}[\dot{W}_{BPMED} + \dot{W}_{blower} + \dot{W}_{comp} + \dot{W}_{pump}] \tag{15}$$

where $\dot{W}_{BPMED}$ is the power consumption of the BPMED process, $\dot{W}_{blower}$ is the energy demand of the air blower, $\dot{W}_{comp}$ is the power demand of the CO_2 compressor, and $\dot{W}_{pump}$ is the power demand of the lean/rich pumps.

Seven optimization variables have been selected for the process adopting the CEM cell configuration:

https://doi.org/10.1021/acs.iecr.2c00889
Ind. Eng. Chem. Res. 2022, 61, 12668−12679

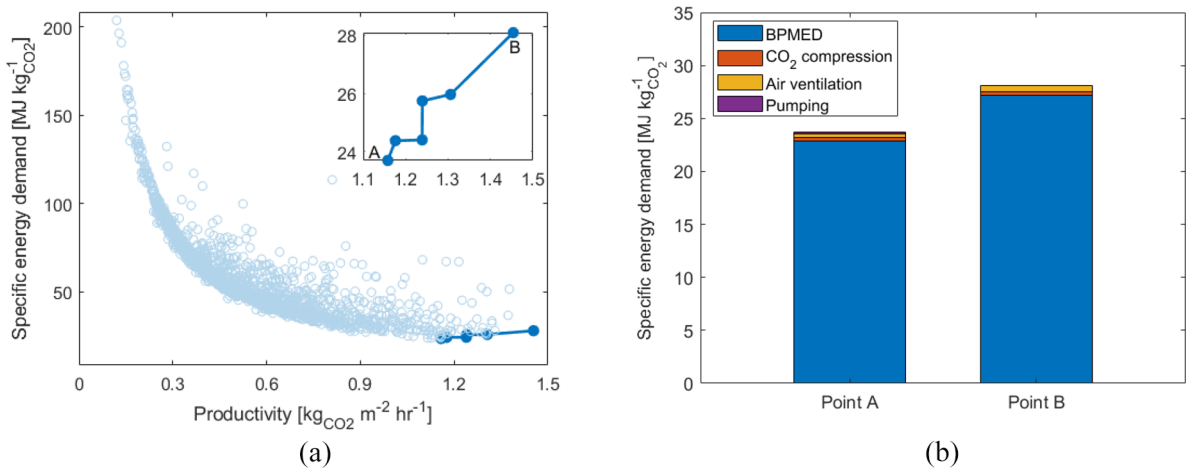

Figure 3. (a) Specific energy demand−productivity plane for the BPM−CEM process. (Inset) Pareto front with point A providing the minimum energy consumption and point B the maximum productivity. Empty points represent suboptimal conditions. (b) Breakdown of the energy demand for points A and B of the Pareto front.

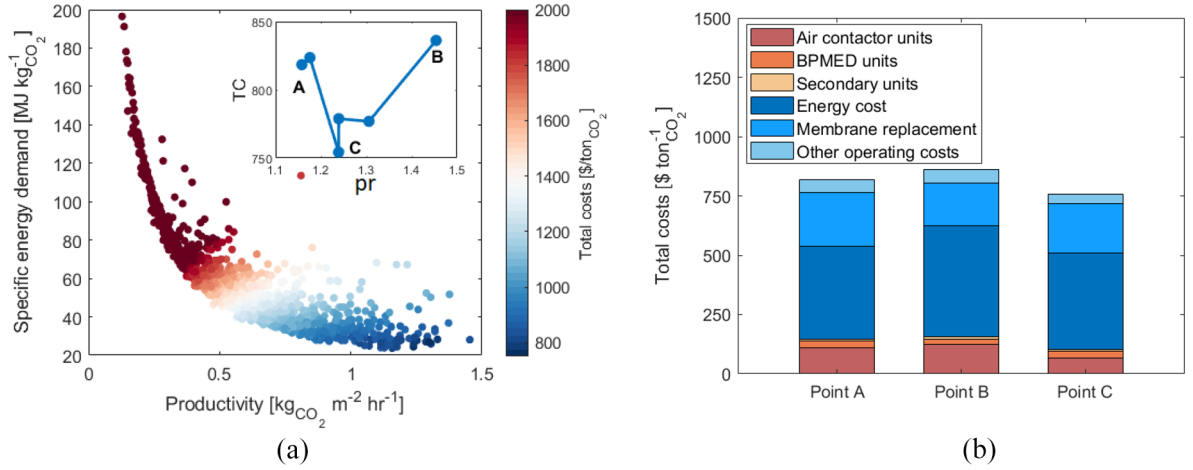

Figure 4. (a) Map of total costs for suboptimal and Pareto points of the BPM−CEM process. (Inset) Total cost (TC) for Pareto points only, with point C providing the lowest possible cost. (b) Breakdown of the total process costs for point A, B, and C of the Pareto front.

- Absorber loading (ξ), defined as the ratio between the number of moles of KOH in the lean stream and the number of moles of CO_2 in the air stream;
- Concentration of KOH in the lean stream (c_{KOH});
- Air velocity in the contactor unit (u_{air});
- Recycle ratio (R_{REC}), the fraction of the rich stream which is recycled back to the air contactor;
- Regeneration ratio (R_{REG}), defined as the ratio between the molar flow rate of K^+ in the rich stream to be regenerated and the ionic flow rate across the BPMED;
- Pressure of the BPMED unit (P_{BPMED});
- Pressure of the knockout vessel (P_{KO});

For the AEM variant, an additional variable is included in the optimization:

- Concentration of H_3PO_4 in the acid stream (c_{acid}).

The decision variables and their respective lower and upper boundaries are reported in Table S1 in the Supporting Information. The optimization is carried out using the nondominated Sorting Genetic Algorithm version II (NSGA-II) as available in Matlab (R2020a). Aspen Plus was directly connected to Matlab through the ActiveX framework, thus making the data exchange and the overall optimization procedure fully automated. Further details can be found in the Supporting Information and in previous works.[19]

Although the BPMED productivity and the overall energy demand have been chosen as objective functions, the process performance is also evaluated through the air contactor productivity, defined as

$$pr_V = \frac{\dot{m}_{CO_2}}{V_{AirContactor}} \tag{16}$$

and the BPMED efficiency, representing the ratio between the recovered CO_2 and the required ion flow rate through the BPMED unit

$$\eta = \frac{\dot{F}_{CO_2}}{J/|z_{CO_3^{2-}}|} \tag{17}$$

Throughout this work, ambient conditions have been assumed to be T = 293 K, p = 1.001 bar, relative humidity of 43%, and CO_2 content of 4×10^{-4}/mol$_{CO2}$/mol.

3. RESULTS

3.1. BPM−CEM Process. *3.1.1. Process Optimization.* The results of the optimization for the BPM−CEM process are

https://doi.org/10.1021/acs.iecr.2c00889
Ind. Eng. Chem. Res. 2022, 61, 12668−12679

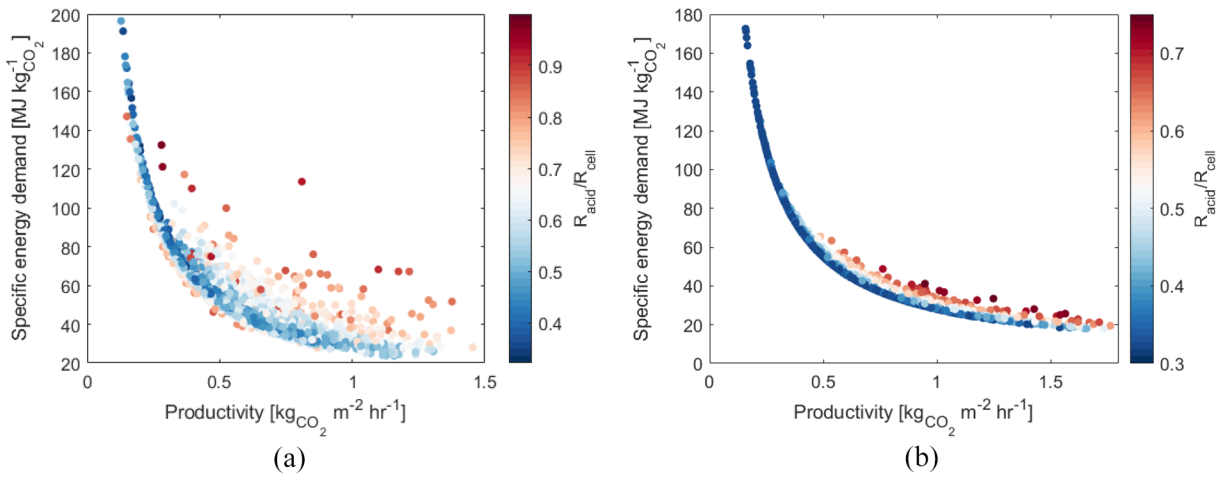

Figure 5. Color maps of the ratio of the acid compartment resistance (R_{acid}) over the total cell resistance (R_{cell}) for (a) the base case and (b) the case of inert salt addition.

shown in Figure 3a. Each point on the *pr*−*e* plane represents a simulation with a specific set of decision variables. The region above the Pareto front, which is located at the bottom right corner, is occupied by suboptimal points, while the region below is unfeasible. Notably, the performance of the process is dramatically affected by the selected decision variables, thus demonstrating the improvement potential of rigorous process optimization.

Figure 4a shows the specific energy demand of the two Pareto extremes. In both cases, the BPMED power consumption is responsible for most of the energy demand and increases with increasing productivity. At point A, the energy demand of the electrodialysis amounts to 22.8 MJ $kg_{CO_2}^{-1}$, which is considerably higher than what was previously reported in the literature for similar processes. Iizuka et al. investigated experimentally the recovery of CO_2 from $NaHCO_3$ solutions at different operating conditions.[13] For a current density of 192 A m^{-2}, an energy demand of 11.5 MJ $kg_{CO_2}^{-1}$ has been measured. The higher *e* reported in this work is due to two reasons. First, a much higher current density has been identified in the optimization, which is required to increase the productivity (and thus reduce the CAPEX). As a consequence, the voltage drop caused by the cell resistance is more substantial. Second, Iizuka et al. carried out experiments using solutions of pure $NaHCO_3$, which is more easily regenerated than the respective carbonate. In a DAC process, however, it is not possible to achieve such a high CO_2 loading in the CO_2-rich streams; thus, only carbonate is present.

Further understanding of the process can be gained by observing the effect of the design variables on the process performance. These results are reported in the Supporting Information. While the absorber loading steadily decreases when moving along the Pareto toward high productivity (Figure S5a), the concentration of KOH in the lean stream tends to increase (Figure S5c). This results in a steep reduction of the lean stream flow rate and a much higher concentration of K_2CO_3 in the rich stream. A high concentration of carbonate is generally favorable for the operation of the BPMED unit. CO_2 is not acidic per se; however, when absorbed into water, it causes the formation of protons according to reactions 1−3. Therefore, as the concentration of HCO_3^- and CO_3^{2-} increases, the pH of the rich stream decreases, thus facilitating the release of CO_2. This is also confirmed by the BPMED efficiency, which rises when moving toward higher productivity (Figure S8c) and ranges between 0.8 and 0.88 for the Pareto points, as the H^+ transport across the CEM is negligible.

However, maximizing productivity comes with costs. With increasing concentration of carbonate in the acid compartment, formation of gas bubbles becomes more and more challenging to avoid. Although the BPMED stack pressure is very close to the upper limit of 30 bar for all of the Pareto points (Figure S6c), the volumetric gas fraction in the acid compartment increases to almost 0.5 when moving toward higher productivity (Figure S8c). For this reason, the cell resistance and therefore power consumption increase with increasing productivity.

A higher energy demand is not the only drawback of higher BPMED efficiency; the extraction of CO_2 from air is also affected. The productivity is enhanced by adjusting the design variables so as to increase the concentration of carbonate in the rich stream; however, this has a detrimental effect on the air contactor productivity (Figure S9) as the capacity of the solvent for absorption is reduced.

3.1.2. Economic Assessment. Figure 4a shows the color map of total costs for both suboptimal and Pareto points of the BPM−CEM process.

Both objectives have a very strong effect on the economics of the process as the cost decreases with increasing productivity and decreasing energy demand. The total costs for the Pareto points range between $757 and $860 $ton_{CO_2}^{-1}$. The high cost is partly due to the conservative values assumed for the cost of membranes, which dominates the process economics. The breakdown reported in Figure 4b reveals that the membranes especially affect the operation and maintenance costs. The short 3 year lifetime assumed for BPMs and IEMs combined with their high price make membrane replacement particularly expensive. Interestingly, the minimum cost is not found at the extremes of the Pareto, i.e., points A and B, but for a point along the Pareto front. As shown in Figure S13c, when moving toward higher productivity, the expenditure related to membranes decreases; on the other hand, the energy demand and its related cost increases, resulting in a marginally higher total process cost. Moreover, in the proximity of the Pareto front, the air contactor significantly affects the process economics. Accordingly, the point that

https://doi.org/10.1021/acs.iecr.2c00889
Ind. Eng. Chem. Res. 2022, 61, 12668−12679

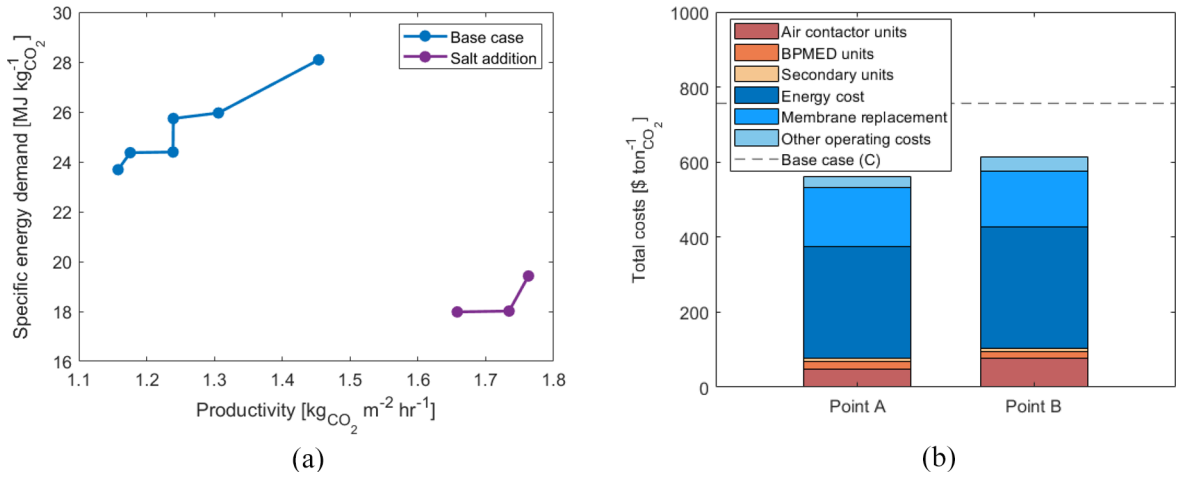

Figure 6. (a) Pareto frontiers for the base case and the salt addition case. (b) Breakdown of the total process costs for points A and B of the Pareto front for the salt addition case. Total cost for point C of the base case is represented as a dotted line.

provides the lowest cost (i.e., point C) features the highest air contactor productivity.

The high cost of the membranes affects not only the capital and maintenance costs but also the energy demand. As explained previously, the current density is selected so as to minimize costs. The effect of this parameter on the process performance and cost has been assessed with a sensitivity analysis, the results of which are reported in Figure S10. With the assumed membrane cost, the optimum is found at a relatively high current density and therefore productivity. Cheaper membranes allow it to operate at a lower current density, thus providing a more energy efficient, albeit less productive, process. For a 10-fold membrane price reduction, a minimum energy demand of 12 MJ $kg_{CO_2}^{-1}$ is found, corresponding to a total process cost of \$367 $ton_{CO_2}^{-1}$.

The cost breakdown clearly shows that the energy accounts for the largest share. Although further reduction of the energy demand through optimization is not possible (for the considered membrane properties), as points below the Pareto front are not feasible, there are additional options to reduce the power consumption of the BPMED unit. The most straightforward is reducing the electrical resistivity of the cell, which directly affects the energy demand (see eqs 7 and 8). We discuss such possible improvements in the next section.

3.1.3. Improved BPM–CEM Cell Resistance by Inert Salt Addition. The BPMED cell resistance is given by the sum of the individual compartment and membrane contributions. Among these, the resistivity of the acid compartment (R_{acid}) is the prevailing one. Figure 5 shows that, in extreme cases, it can account for more than 90% of the overall cell resistance.

The effect of R_{acid} over the cell resistance and its energy demand was also observed by Jiang et al.[27] The poor conductivity of the acid compartment is mostly due to two reasons: the low concentration of electrolytes and the release of gaseous CO_2.[14] While the latter can be in part tackled by increasing the operating pressure of the BPMED unit, the former is an unavoidable consequence of the cell design and thus cannot be improved by simply adjusting the design variables. Most of the K^+ ions are transferred from the acid to the base compartment, while the carbon-containing anions are converted to dissolved CO_2. This effect could be counteracted by adding another salt to the alkali solvent solution. This salt should be inert, meaning that it should not affect the pH of the solution nor the efficiency of the BPMED (i.e., its resulting cation should not be transferred across the CEM). If these requirements are met, addition of this salt would only improve the conductivity of both the acid and the base compartments. The benefits of this approach have been assessed here by varying the conductivity of the electrolyte solutions. It is assumed that the inert salt provides a constant contribution k_{IS} to the electrical conductivity. Therefore, in this case, eq 10 changes to

$$K = k_{IS} + \sum_{i}^{n} k_i \tag{18}$$

where k_{IS} is equal to 15 S m^{-1}, a value comparable with the conductivity of a diluted solution of a strong electrolyte. As a low salt concentration would be required to achieve such conductivity and given the high solubility of KOH and K_2CO_3 in water, the salting out effect is ignored.

The corresponding Pareto fronts for the base case and the salt addition case are reported in Figure 6a.

The improved conductivity obtained with inert salt addition has a considerable effect on the process performance. While the reduction of the specific energy demand was expected, the increase in productivity is surprising, and the reason is found in the new set of operating variables identified by the optimization (see Figure S12). The lower cell resistance makes operation at higher current densities economically viable, thus enabling a higher productivity of the BPMED unit. Although the acid compartment resistivity greatly benefits from salt addition, it still accounts for 20–40% of the total cell resistance (Figure S12d). This is due to the high volumetric gas fractions found in the acid compartment (Figure S12c), which affect its conductivity. The presence of the inert salt has also another effect, as shown in Figure S13c. The concentration of KOH in the lean stream is substantially lower in the salt addition case, as c_{KOH} no longer plays an important role in improving the cell conductivity.

The improvement in performance benefits the economics of the process. The cost breakdown for points A and B for the salt addition case is reported in Figure 6b. At the Pareto, the total cost varies between \$561 and \$614 $ton_{CO_2}^{-1}$, which is 26–29% lower than the costs estimated for the base case. Interestingly, the presence of the inert salt enhances not only the solvent

https://doi.org/10.1021/acs.iecr.2c00889
Ind. Eng. Chem. Res. 2022, 61, 12668–12679

regeneration but also the capture of CO_2. Salt addition enables operation of the air contactor at more favorable conditions. The levelized cost of the air capture units is \$49−77 $ton_{CO_2}^{-1}$, a 56−38% reduction compared to the base case. The regeneration ratio is much higher when the inert salt is included (Figure S14b), meaning that more CO_2 is recovered and therefore a leaner solvent with a higher absorption capacity is obtained. Thus, the air contactor achieves a higher productivity, reducing the total volume required.

3.1.4. Improved BPM−CEM Cell Resistance by Enhanced Membrane Conductivity. The increasing interest in IEMs and BPMs is providing many advancements in terms of materials and preparation techniques.[28] It is reasonable to expect that in the coming years membranes with improved stability and performance will become available at a lower price than what is currently present on the market. For CEMs, the electrical conductivity is the most critical parameter as selectivity is not an issue. Membranes provide the second biggest contribution to the BPMED cell resistance; therefore, there is a clear incentive to explore the effect of their resistivity on the operation of the DAC process. Here, we do so via a sensitivity analysis on the membrane conductivity. In this way, we also aim at providing an assessment of how membrane development could improve the efficiency of the processes. The results are reported in Figure 7.

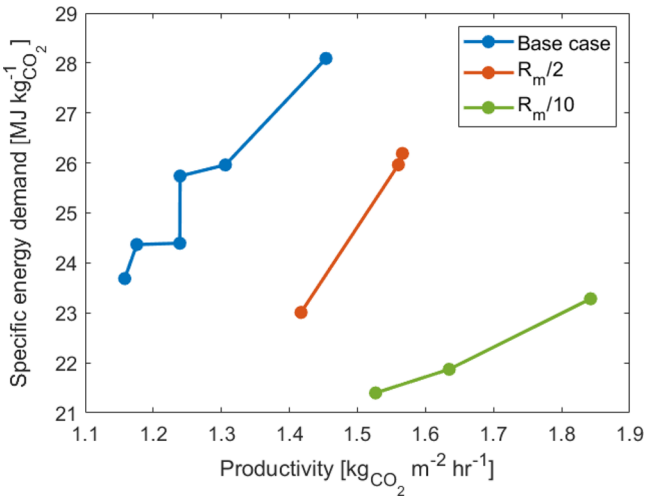

Figure 7. Pareto frontiers for the base case, membrane resistivity reduced by a factor 2 ($R_m/2$), and membrane resistivity reduced by a factor 10 ($R_m/10$).

The specific energy demand and productivity improve with decreasing membrane resistivity, although only incrementally. As explained in the previous section, the acid compartment generally has the highest electrical resistance, meaning that R_m does not drastically affect the performance. Further understanding can be gained by inspecting the operating conditions along the Pareto (see Figure S16). Current density and therefore productivity tend to rise for lower membrane resistivity, since the improvement in cell conductivity shifts the economic optimum to higher current densities. R_m has an effect on the volumetric gas fraction in the acid compartment as well, which decreases for the $R_m/2$ case and even further for $R_m/10$. While the air velocity and lean composition remain similar, the absorber loading tends to increase for the cases with reduced membrane resistivity (see Figure S17). As a consequence, the concentration of carbonate in the rich stream for the $R_m/2$ and $R_m/10$ cases is lower, thus reducing the release of CO_2 in the gas phase.

The membrane conductivity also affects the CO_2 capture. The levelized cost of the air contactor is reduced for the cases with lower membrane resistance (\$68−75 $ton_{CO_2}^{-1}$ for $R_m/2$ and \$86−90 $ton_{CO_2}^{-1}$ for $R_m/10$; see Figure S19). Similar to what was observed in the previous section, improving the conductivity of the cell relaxes the constraints on the BPMED unit, allowing for a more efficient CO_2 capture.

3.2. BPM−AEM Process. *3.2.1. Process Optimization.* Figure 8a shows the suboptimal and Pareto points obtained from the optimization of the BPM−AEM process. Again, rigorous process optimization enhances the process performance significantly. It is also evident that the BPM−AEM cell configuration provides poorer results when compared to its CEM counterpart. Specifically, the minimum energy demand (i.e., point A of the Pareto) is almost 1.9 times higher, while the maximum productivity (i.e., point B of the Pareto) is approximately 2.2 times lower. As reported in Figure 8b, the increased energy consumption is only attributable to BPMED, which at point A contributes 43 MJ $kg_{CO_2}^{-1}$. These results can be compared with the experimental work of Eisaman et al.[11] For a solution containing 0.5 mol L^{-1} K_2CO_3 and 0.1 mol L^{-1} KOH, Eisaman measured an energy demand of 79.5 MJ $kg_{CO_2}^{-1}$ at 800 A m^{-2}. The higher energy requirement is due to higher concentration of KOH and overall low concentration of electrolyte species. Using the data published by Eisaman, we estimated in our previous work a minimum energy demand of 21.75 MJ $kg_{CO_2}^{-1}$.[17] This result was obtained assuming a BPMED efficiency ranging between 80% and 90%. However, we show here that η could only be as high as 37% (see Figure S25).

On the other hand, the different cell configuration does not significantly affect the operation of the process. The resulting operating conditions at the Pareto are in the same range as for the BPM−CEM system (see Figures S21 and S22).

For the Pareto points, the efficiency of BPMED varies between 0.34 and 0.375 (Figure S25), while for the BPM−CEM cell configuration, η ranged from 0.80 to 0.88 (Figure S7). This considerable difference is caused by the relatively high concentration of OH^- in the base compartment and the different values adopted for the permselectivity of CEMs and AEMs. Both OH^- and H^+ have exceptional mobility in both electrolyte solutions and membranes due to their peculiar transport mechanism. Therefore, they exhibit much faster transfer rates than other ions.[22] However, while the concentration of protons in the acid compartment of the BPM−CEM cell is negligible, there is a significant concentration of OH^- in the base compartment of the BPM−AEM cell. Therefore, hydroxide makes for a substantial fraction of the ions transported across the AEM (Figure S26). The transfer of ions not carrying CO_2 is a waste of energy and membrane area, thus explaining the poor performance of this configuration.

3.2.2. Economic Assessment. As expected, the worse process performance adversely affects the economics. Figure 9a shows that there are no points for which the total cost falls below \$1000 $ton_{CO_2}^{-1}$. The process cost features a strong dependence on productivity and even more on energy demand.

https://doi.org/10.1021/acs.iecr.2c00889
Ind. Eng. Chem. Res. 2022, 61, 12668−12679

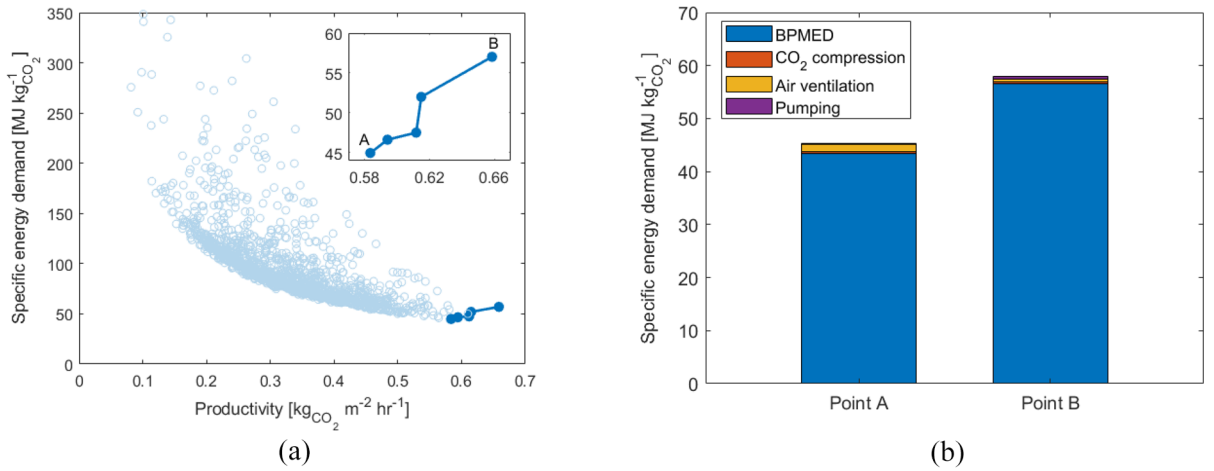

Figure 8. (a) Specific energy demand−productivity plane for the BPM−AEM process. (Inset) Pareto front, with point A providing the minimum energy consumption and point B the maximum productivity. Empty points represent suboptimal conditions. (b) Breakdown of the energy demand for points A and B of the Pareto front.

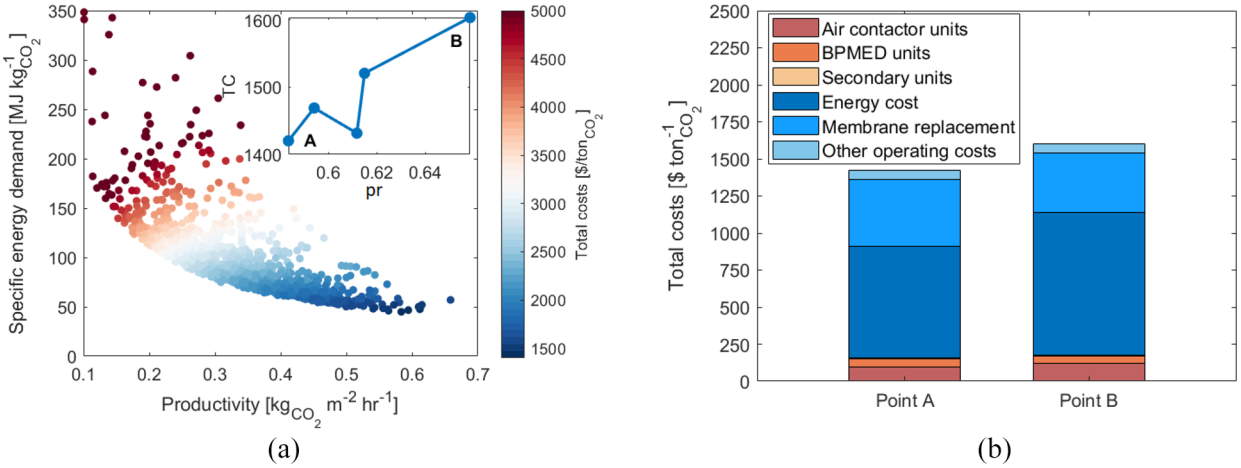

Figure 9. (a) Map of total costs for suboptimal and Pareto points of the BPM−AEM process. (Inset) Total cost (TC) for Pareto points only. (b) Breakdown of the total process costs for points A and B of the Pareto front.

At the Pareto, the cost steadily increases with increasing productivity from \$1420 to \$1604 ton$_{CO_2}^{-1}$.

The cost breakdown reported in Figure 9b confirms the importance of the energy consumption, as electricity accounts for the largest share of the total levelized expenditure. The acid compartment contributes to a large part of the cell resistance, albeit to a lesser extent than in the BPM−CEM configuration. Indeed, the relatively high concentration of H_3PO_4 in the acid solution partially makes up for the release of gaseous CO_2, an issue that also affects this process configuration. However, as previously explained, the main limitation of the BPM−AEM cell is the significant transport of OH^-.

3.2.3. Improved Membrane Selectivity. Ion selectivity is a key feature of electrochemical separations.[22] Several methods to improve the selectivity of AEMs have been reported, with surface modifications being the most researched.[29] This technology usually comes at the cost of higher membrane resistance and therefore energy demand. Moreover, hindering the transport of OH^- is very challenging, as hydroxide has extremely high mobility in AEMs due to its small radius. For this analysis and with the aim of determining the full potential of such configuration, we will neglect these aspects and assume that the selectivity toward CO_3^{2-} could be enhanced without consequences for the conductivity of the membrane. Two additional cases are examined: a conservative one in which the selectivity is only increased by a factor of 2 ($2P_m$) and a more optimiztic case in which a factor of 10 is adopted ($10P_m$). The resulting Pareto fronts are reported in Figure 10.

A relatively small improvement of a factor 2 in the membrane selectivity ($2P_m$) is not enough to push the process performance further, while the $10P_m$ case offers a significant increase in productivity and reduction of energy demand. In fact, there is little difference in terms of OH^- transfer between the base case and the case of $2P_m$ (see Figure S28). In these instances, the concentration of hydroxide in the base compartment is the limiting factor and the membrane selectivity is not able to influence the composition of the ion flow across the AEM. The considerable advancement assumed in $10P_m$, however, determines a decrease of the molar fraction of OH^- from 0.61−0.63 to 0.28−0.35. The improved selectivity is the only cause for the improved performance, as there are no significant differences in the resulting design variables at the Pareto front for the three cases (see Figures S29 and S30). The results of the economic analysis for these cases are reported in Figure S31. As expected, the $2P_m$ case provides no economic benefit, while the costs for the $10P_m$ case

https://doi.org/10.1021/acs.iecr.2c00889
Ind. Eng. Chem. Res. 2022, 61, 12668−12679

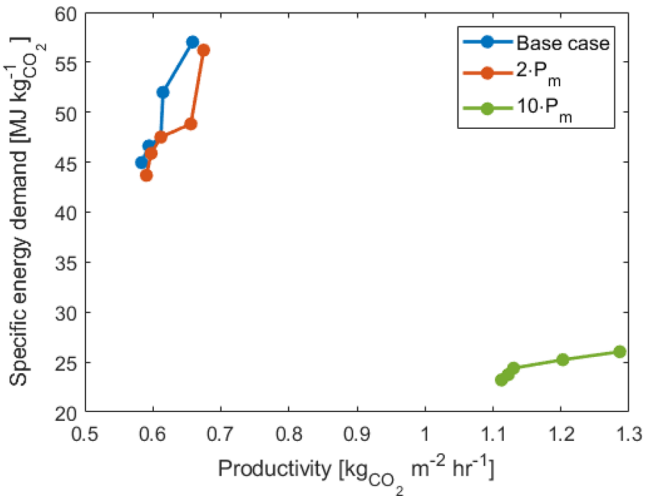

Figure 10. Pareto frontiers for the base case, membrane selectivity increased by a factor 2 ($2P_m$), and membrane selectivity increased by a factor 10 ($10P_m$).

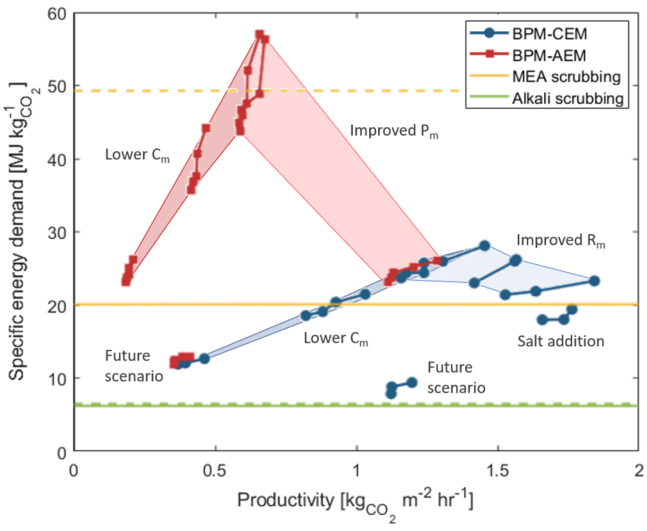

Figure 11. Resulting Pareto fronts for all cases considered. Energy demand for point A (solid line) and point B (dotted line) of the Pareto for the MEA scrubbing process and the alkali scrubbing process from Sabatino et al.[19] For future scenarios, we assume a 10-fold increase in either membrane conductivity (BPM−CEM) or selectivity (BPM−AEM), a 10-fold reduction in membrane cost, and addition of an inert salt.

are significantly lower at \$784−801 $ton_{CO_2}^{-1}$. This is lower than what was estimated for the base case of the BPM−CEM configuration. In part, this outcome is due to the better conductivity of the BPM−AEM cell and the ensuing lower energy demand, but the primary cause lies elsewhere. Although OH^- leakage is still noteworthy in the $10P_m$ case, the BPMED efficiency achieved at the Pareto is very close to what has been determined for the BPM−CEM alternative (Figure S32). Employing a designated acid solution to recover carbon dioxide is a more robust and efficient design, as it is not relying on the pH of neither the CO_2-rich nor the CO_2-lean stream. Therefore, if a significant improvement in membrane technology would be achieved in the coming years, the BPM−AEM configuration process could certainly compete with the BPM−CEM alternative.

4. BPMED PROCESS BENCHMARK AND DISCUSSION

The suitability of BPMED for the regeneration step in DAC processes should also be assessed by comparing it to alternative technologies. From this perspective, two absorption-based processes stand out in light of their technological readiness or widespread employment, namely, the alkali-scrubbing process developed by Carbon Engineering and the liquid-scrubbing process via alkanolamines. In a previous work,[19] both technologies were modeled and optimized, although using the air contactor productivity pr_V as objective function. In Figure 11, the Pareto fronts of all of the cases considered for both BPM−CEM and BPM−AEM configurations are reported together with the estimated energy demands for these two benchmark technologies. An overview of the cases considered in this work and their estimated total cost is reported in Table S5 in the Supporting Information.

BPMED competes with a mature process like amine scrubbing, and the BPM−CEM cell configuration process could outperform it provided that cheaper membranes would be available or more advanced process designs (e.g., inert salt addition) could be adopted. A 2-fold reduction in membrane cost would already place the minimum energy demand below 20 MJ $kg_{CO_2}^{-1}$, which is the lowest estimated energy consumption for the amine-based process. However, the thermochemical regeneration process developed by Carbon Engineering performs better at 6.21 MJ $kg_{CO_2}^{-1}$. To abate the energy demand to this level, several improvements to the BPM−CEM cell configuration process should be introduced. A 10-fold reduction in membrane cost and resistance combined with inert salt addition would lower the energy demand to 7.9 MJ $kg_{CO_2}^{-1}$ (future scenario in Figure 11).

The better performance also affects the economics of the process. In this scenario, a total cost of \$241 $ton_{CO_2}^{-1}$ is estimated, which is very close to the \$232 $ton_{CO_2}^{-1}$ reported by Keith et al. for Carbon Engineering's process.[5] Two main reasons can be identified for the higher costs of the BPMED process: the worse air contactor performance and the more expensive energy source. As explained in the Results section, optimization of the electrodialysis unit is carried out at the expense of CO_2 capture efficiency. For the BPM−CEM cell configuration process, the air contactor productivity ranges between 0.18 and 0.23 $kg_{CO_2}\ m^{-3}\ h^{-1}$ at the Pareto. Using the same methodology, we reported values of 0.18−0.45 and 0.75−1.08 $kg_{CO_2}\ m^{-3}\ h^{-1}$ for the alkali- and amine-scrubbing processes, respectively.[19] This has implications also on the economics. Keith et al. estimated that the air contactor would contribute \$46 $ton_{CO_2}^{-1}$ to the total process cost, while for the BPMED processes, this figure is generally more than doubled. Moreover, most of the energy required by the thermochemical regeneration technology is provided in the form of (cheap) natural gas, while for electrodialysis, more expensive electricity is required. However, for the past decade, the levelized cost of energy (LCOE) of electricity generated from renewable sources has been steadily decreasing.[30] The benefits provided by cheaper renewable energy to BPMED processes have been assessed with a sensitivity analysis on the electricity cost, the results of which are reported in Figure S20. Besides lower operating costs, cheaper electricity would also allow it to operate at an even higher current density and therefore productivity. In the case of using photovoltaic panels, which

https://doi.org/10.1021/acs.iecr.2c00889
Ind. Eng. Chem. Res. 2022, 61, 12668−12679

are estimated to have an LCOE as low as \$0.02 kWh^{-1} by 2030,[31] the total cost would decrease to \$515 $ton_{CO_2}^{-1}$ for the base-case BPM−CEM cell configuration process.

The formation of CO_2 bubbles inside the BPMED cell can drastically affect the energy demand of the process. We have shown that operation at a pressure of 20−30 bar can partly overcome this issue, but in these conditions, the solubility of carbon dioxide in water is still limited. Alternative process line ups could provide better results. Valluri et al. proposed a process in which the recovery of CO_2 and the regeneration of the sorbent through electrodialysis are carried out in different steps.[15] First, the $NaHCO_3$ absorbent solution is reacted with H_2SO_4, thus lowering its pH and causing the release of CO_2. The resulting Na_2SO_4 solution is then fed to a BPM−CEM cell electrodialysis unit, from which both the acid and the NaOH solvent are recovered. The authors have measured energy demands as low as 1.18 MJ $kg_{CO_2}^{-1}$ for postcombustion applications, making this an interesting concept for DAC too.

5. CONCLUSIONS

With this work, we have thoroughly assessed the applicability of bipolar membrane electrodialysis in two configurations (viz., BPM−CEM and BPM−AEM) for the recovery of CO_2 in DAC processes. The results have shown that through rigorous optimization, the performance of both processes can be drastically improved. A minimum energy demand of 24 MJ $kg_{CO_2}^{-1}$ has been estimated for the BPM−CEM cell configuration process, which is similar to what has been reported for other liquid-scrubbing DAC technologies, e.g., amine scrubbing. However, this is significantly higher than the thermochemical energy required in the process developed by Carbon Engineering. The AEM alternative, moreover, suffers from the poor selectivity of current ion-exchange membranes. For this process, we predict an energy demand of 45 MJ $kg_{CO_2}^{-1}$. Our results show that only a 10-fold improvement in selectivity would allow the BPM−AEM cell configuration process to compete with the BPM−CEM option.

The economic assessment has shown that the energy cost is the biggest expense; therefore, we have explored solutions to improve the cell conductivity and thus reduce the power consumption of BPMED. One such approach is the addition of an inert salt to the solvent solution in order to increase the concentration of electrolyte species and thus the electric conductivity. In this way, the energy demand of the BPM−CEM cell configuration process can be reduced to 17 MJ $kg_{CO_2}^{-1}$. Further developments should be aimed at improving the electrical conductivity and overall stability of ion-exchange membranes as the power consumption of BPMED and membrane replacement have a considerable weight on the process economics. In our future scenario, where cheaper and more durable membranes are assumed to be available, total costs below \$250 $ton_{CO_2}^{-1}$ may become feasible for the BPM−CEM cell configuration process, making it a viable fully electrified alternative to the thermochemical regeneration of the Carbon Engineering technology that requires natural gas.

ASSOCIATED CONTENT

Supporting Information

The Supporting Information is available free of charge at https://pubs.acs.org/doi/10.1021/acs.iecr.2c00889.

Additional details regarding the modeling methodology and results (PDF)

AUTHOR INFORMATION

Corresponding Author

Francesco Sabatino − *Department of Chemical Engineering and Chemistry, Technische Universiteit Eindhoven, Eindhoven 5600 MB, The Netherlands;* orcid.org/0000-0002-9218-1587; Email: f.sabatino@tue.nl

Authors

Matteo Gazzani − *Copernicus Institute of Sustainable Development, Universiteit Utrecht, Utrecht 3584 CB, The Netherlands;* orcid.org/0000-0002-1352-4562

Fausto Gallucci − *Department of Chemical Engineering and Chemistry, Technische Universiteit Eindhoven, Eindhoven 5600 MB, The Netherlands*

Martin van Sint Annaland − *Department of Chemical Engineering and Chemistry, Technische Universiteit Eindhoven, Eindhoven 5600 MB, The Netherlands;* orcid.org/0000-0002-2903-7443

Complete contact information is available at: https://pubs.acs.org/10.1021/acs.iecr.2c00889

Notes

The authors declare no competing financial interest.

ACKNOWLEDGMENTS

This work was sponsored by Shell Global Solutions International BV.

REFERENCES

(1) Tollefson, J. COVID curbed carbon emissions in 2020 - but not by much. *Nature* **2021**, *589*, 343.

(2) Hanna, R.; Abdulla, A.; Xu, Y.; Victor, D. G. Emergency deployment of direct air capture as a response to the climate crisis. *Nat. Commun.* **2021**, *12*, 368.

(3) Sanz-Pérez, E. S.; Murdock, C. R.; Didas, S. A.; Jones, C. W. Direct Capture of CO2 from Ambient Air. *Chem. Rev.* **2016**, *116*, 11840−11876.

(4) Zeman, F. Energy and material balance of CO2 capture from ambient air. *Environ. Sci. Technol.* **2007**, *41*, 7558−7563.

(5) Keith, D. W.; Holmes, G.; St. Angelo, D.; Heidel, K. A Process for Capturing CO2 from the Atmosphere. *Joule* **2018**, *2*, 1573−1594.

(6) Li, T.; Keener, T. C. A review: Desorption of CO2 from rich solutions in chemical absorption processes. *Int. J. Greenh. Gas Control* **2016**, *51*, 290−304.

(7) Sharifian, R.; Wagterveld, R. M.; Digdaya, I. A.; Xiang, C.; Vermaas, D. A. Electrochemical carbon dioxide capture to close the carbon cycle. *Energy Environ. Sci.* **2021**, *14*, 781−814.

(8) Butler, J. N. *Carbon Dioxide Equilibria their Applications*, 1st ed.; Routledge: New York, 2019; p 272.

(9) Shu, Q.; Legrand, L.; Kuntke, P.; Tedesco, M.; Hamelers, H. V. Electrochemical Regeneration of Spent Alkaline Absorbent from Direct Air Capture. *Environ. Sci. Technol.* **2020**, *54*, 8990−8998.

(10) Zhou, C.; Ni, J.; Chen, H.; Guan, X. Harnessing electrochemical pH gradient for direct air capture with hydrogen and oxygen by-products in a calcium-based loop. *Sustain. Energy Fuels* **2021**, *5*, 4355−4367.

(11) Eisaman, M. D.; Alvarado, L.; Larner, D.; Wang, P.; Garg, B.; Littau, K. A. CO2 separation using bipolar membrane electrodialysis. *Energy Environ. Sci.* **2011**, *4*, 1319−1328.

(12) Eisaman, M. D.; Parajuly, K.; Tuganov, A.; Eldershaw, C.; Chang, N.; Littau, K. A. CO2 extraction from seawater using bipolar membrane electrodialysis. *Energy Environ. Sci.* **2012**, *5*, 7346−7352.

(13) Iizuka, A.; Hashimoto, K.; Nagasawa, H.; Kumagai, K.; Yanagisawa, Y.; Yamasaki, A. Carbon dioxide recovery from carbonate solutions using bipolar membrane electrodialysis. *Sep. Purif. Technol.* **2012**, *101*, 49−59.
(14) Eisaman, M. D.; Alvarado, L.; Larner, D.; Wang, P.; Littau, K. A. CO2 desorption using high-pressure bipolar membrane electrodialysis. *Energy Environ. Sci.* **2011**, *4*, 4031.
(15) Valluri, S.; Kawatra, S. K. Reduced reagent regeneration energy for CO2 capture with bipolar membrane electrodialysis. *Fuel Process. Technol.* **2021**, *213*, 106691.
(16) Nagasawa, H.; Yamasaki, A.; Iizuka, A.; Kumagai, K.; Yanagisawa, Y. A new recovery process of carbon dioxide from alkaline carbonate solution via electrodialysis. *AIChE J.* **2009**, *55*, 3286−3293.
(17) Sabatino, F.; Mehta, M.; Grimm, A.; Gazzani, M.; Gallucci, F.; Kramer, G. J.; van Sint Annaland, M. Evaluation of a Direct Air Capture Process Combining Wet Scrubbing and Bipolar Membrane Electrodialysis. *Ind. Eng. Chem. Res.* **2020**, *59*, 7007−7020.
(18) Mehmood, A.; Iqbal, M. I.; Lee, J. Y.; Hwang, J.; Jung, K. D.; Ha, H. Y. A novel high performance configuration of electrochemical cell to produce alkali for sequestration of carbon dioxide. *Electrochim. Acta* **2016**, *219*, 655−663.
(19) Sabatino, F.; Grimm, A.; Gallucci, F.; van Sint Annaland, M.; Kramer, G. J.; Gazzani, M. A comparative energy and costs assessment and optimization for direct air capture technologies. *Joule* **2021**, *5*, 2047−2076.
(20) Holmes, G.; Keith, D. W. An air-liquid contactor for large-scale capture of CO 2 from air. *Philos. Trans. R. Soc. A Math. Phys. Eng. Sci.* **2012**, *370*, 4380−4403.
(21) Holmes, G.; Nold, K.; Walsh, T.; Heidel, K.; Henderson, M. A.; Ritchie, J.; Klavins, P.; Singh, A.; Keith, D. W. Outdoor prototype results for direct atmospheric capture of carbon dioxide. *Energy Procedia* **2013**, *37*, 6079−6095.
(22) Luo, T.; Abdu, S.; Wessling, M. Selectivity of ion exchange membranes: A review. *J. Membr. Sci.* **2018**, *555*, 429−454.
(23) Tanaka, Y. *Ion Exchange Membranes*, 2nd ed.; Elsevier, 2015; Chapter 17, pp 369−392.
(24) Gilliam, R. J.; Graydon, J. W.; Kirk, D. W.; Thorpe, S. J. A review of specific conductivities of potassium hydroxide solutions for various concentrations and temperatures. *Int. J. Hydrogen Energy* **2007**, *32*, 359−364.
(25) Meredith, R. E.; Tobias, C. W. Conductivities in Emulsions. *J. Electrochem. Soc.* **1961**, *108*, 286.
(26) Kiani, A.; Jiang, K.; Feron, P. Techno-Economic Assessment for CO2 Capture From Air Using a Conventional Liquid-Based Absorption Process. *Front. Energy Res.* **2020**, *8*, 92.
(27) Jiang, C.; Li, S.; Zhang, D.; Yang, Z.; Yu, D.; Chen, X.; Wang, Y.; Xu, T. Mathematical modelling and experimental investigation of CO2 absorber recovery using an electro-acidification method. *Chem. Eng. J.* **2019**, *360*, 654−664.
(28) Ran, J.; Wu, L.; He, Y.; Yang, Z.; Wang, Y.; Jiang, C.; Ge, L.; Bakangura, E.; Xu, T. Ion exchange membranes: New developments and applications. *J. Membr. Sci.* **2017**, *522*, 267−291.
(29) Khoiruddin; Ariono, D.; Subagjo; Wenten, I. G. Surface modification of ion-exchange membranes: Methods, characteristics, and performance. *J. Appl. Polym. Sci.* **2017**, *134*, 45540.
(30) *Renewable Power Generation Costs in 2020*; IRENA, 2021.
(31) Cole, W.; Frew, B.; Gagnon, P.; Richards, J.; Sun, Y.; Zuboy, J.; Woodhouse, M.; Margolis, R. *SunShot 2030 for Photovoltaics (PV): Envisioning a Low-cost PV Future*; U.S. Department of Energy, 2017.

https://doi.org/10.1021/acs.iecr.2c00889
Ind. Eng. Chem. Res. 2022, 61, 12668−12679